# Morphology of diesel soot residuals from supercooled water droplets and ice crystals: implications for optical properties



2015 Environ. Res. Lett. 10 114010

(http://iopscience.iop.org/1748-9326/10/11/114010)

Environmental Research Letters

LETTER

# Morphology of diesel soot residuals from supercooled water droplets and ice crystals: implications for optical properties

**Swarup China**[1,2,9], **Gourihar Kulkarni**[3], **Barbara V Scarnato**[4], **Noopur Sharma**[1], **Mikhail Pekour**[3], **John E Shilling**[3], **Jacqueline Wilson**[5], **Alla Zelenyuk**[5], **Duli Chand**[3], **Shang Liu**[6,7], **Allison C Aiken**[6], **Manvendra Dubey**[6], **Alexander Laskin**[8], **Rahul A Zaveri**[3] **and Claudio Mazzoleni**[1,9]

[1] Atmospheric Sciences Program and Physics Department, Michigan Technological University, Houghton MI, USA
[2] Now at: Environmental Molecular Sciences Laboratory, Pacific Northwest National Laboratory, Richland WA, USA
[3] Atmospheric Sciences and Global Change Division, Pacific Northwest National Laboratory, Richland WA, USA
[4] Department of Meteorology, Naval Postgraduate School, Monterey CA, USA
[5] Chemical Physics and Analysis, Pacific Northwest National Laboratory, Richland WA, USA
[6] Earth and Environmental Sciences Division, Los Alamos National laboratory, Los Alamos NM, USA
[7] Now at: Cooperative Institute for Research in Environmental Sciences and Department of Chemistry and Biochemistry, University of Colorado, Boulder CO, USA
[8] Environmental Molecular Sciences Laboratory, Pacific Northwest National Laboratory, Richland WA, USA
[9] Authors to whom any correspondence should be addressed.

**E-mail:** schina@mtu.edu **and** cmazzoleni@mtu.edu

**Keywords:** soot, morphology, ice cloud processing, optical properties, radiative forcing

Supplementary material for this article is available online

OPEN ACCESS

RECEIVED
14 August 2015

REVISED
30 September 2015

ACCEPTED FOR PUBLICATION
16 October 2015

PUBLISHED
4 November 2015



## Abstract

Freshly emitted soot particles are fractal-like aggregates, but atmospheric processes often transform their morphology. Morphology of soot particles plays an important role in determining their optical properties, life cycle and hence their effect on Earth's radiative balance. However, little is known about the morphology of soot particles that participated in cold cloud processes. Here we report results from laboratory experiments that simulate cold cloud processing of diesel soot particles by allowing them to form supercooled droplets and ice crystals at −20 and −40 °C, respectively. Electron microscopy revealed that soot residuals from ice crystals were more compact (roundness ∼0.55) than those from supercooled droplets (roundness ∼0.45), while nascent soot particles were the least compact (roundness ∼0.41). Optical simulations using the discrete dipole approximation showed that the more compact structure enhances soot single scattering albedo by a factor up to 1.4, thereby reducing the top-of-the-atmosphere direct radiative forcing by ∼63%. These results underscore that climate models should consider the morphological evolution of soot particles due to cold cloud processing to improve the estimate of direct radiative forcing of soot.

## 1. Introduction

Soot particles consist of aggregates of many spherical carbonaceous monomers (spherules) and are ubiquitous in the atmosphere. Soot particles are directly emitted into the atmosphere from a variety of combustion sources (Streets *et al* 2004). While fossil fuels (e.g., diesel, gasoline, oil, coal) combustion and open biomass burning at the ground level emit soot into the boundary layer, aviation emits it directly in the upper troposphere (Kärcher *et al* 1998, Wang 2011, Schumann *et al* 2013). Soot particles can also be transported from the boundary layer to the upper troposphere by deep convection (Storelvmo 2012). Soot particles affect climate directly by absorbing and scattering sunlight and indirectly by serving as a cloud condenstaion nuclei or ice nuclei (IN) (Bond *et al* 2013). Soot deposited on snow and ice sheets can decrease the surface albedo, thereby accelerating melting (Hansson and Ahlberg 1985, Ramanathan and Carmichael 2008). Furthermore, soot particles can increase absorption of solar radiation by decreasing cloud cover in the lower troposphere (Lohmann and Feichter 2005). Soot particles incorporated within ice crystals and droplets

in clouds can also enhance light absorption and decrease cloud albedo (Hansen and Nazarenko 2004, Jacobson 2006, Ramanathan and Carmichael 2008).

At supercooled temperatures of the upper troposphere, soot particles can facilitate formation of ice clouds through heterogenous ice nucleation mechanisms (Demott 1990, Diehl and Mitra 1998, Gorbunov *et al* 2001, Kärcher *et al* 2007, Fornea *et al* 2009, Crawford *et al* 2011). The efficiency of soot as an IN depends on various parameters such as temperature, relative humidity, supersaturation, soot size, surface oxidation and ice active sites (DeMott *et al* 1999, Gorbunov *et al* 2001, Persiantseva *et al* 2004, Möhler *et al* 2005, DyMarska *et al* 2006, Hoose and Möhler 2012). Aircraft soot emissions play a major role in contrail fomation in the upper troposphere at −40 °C or below (Kärcher *et al* 1998) and induce ice formation in contrails (Petzold *et al* 1999).

Twohy and Poellot (2005) investigated ice crystal residual particles from cirrus clouds and showed that 11%–25% of the residuals are composed of carbonaceous material, including soot and organic carbon. Petzold *et al* (1998) observed higher soot number concentration (0.2 $cm^{-3}$) in ice crystal residuals from contrail compared to cirrus (0.02 $cm^{-3}$). They suggsted that soot in the cirrus cloud can be attributed to scavenging of soot by ice crystals. They found that contrail residues are dominated (87%) by small soot particles (<200 nm) mostly composed of carbon and only a minor fraction (1.6%) of larger soot particles (∼1000 nm) that were coated with sulfate. Targino *et al* (2006) found a small fraction of soot in individual ice crystal residues from orographic wave clouds. Several other studies also found a small fraction of soot in cirrus ice crystal residues (Cziczo *et al* 2013, Cziczo and Froyd 2014). Furthermore, a recent study found compact soot particles in Antarctic ice core samples (Ellis *et al* 2015).

Freshly emitted soot particles are typically lacy fractal-like aggregates, but change their morphology during transport via various aging process. For example, compact soot particles are abundant in the free troposphere of a remote marine region in the North Atlantic (China *et al* 2015). The morphology of soot particles significantly influence their optical properties (Liu *et al* 2008, Scarnato *et al* 2013, Radney *et al* 2014, China *et al* 2015). Modeling studies showed that the scattering, absorption and extinction (scattering + absorption) cross sections of soot change upon restructuring depending on the refractive index, the monomer diameter and the structural details (Liu *et al* 2008, Kahnert and Devasthale 2011, Scarnato *et al* 2013, Radney *et al* 2014, China *et al* 2015).

Warm cloud droplets containing soot particles can experience several cycles of condensation and evaporation (Huang *et al* 1994). Such cloud processing plays a key role in compacting (restructuring) the soot fractal-like aggregates (Khalizov *et al* 2013), thereby altering their optical properties (Colbeck *et al* 1990, Mikhailov *et al* 2006, Lewis *et al* 2009, Radney *et al* 2014, China *et al* 2015). Previous studies (Huang *et al* 1994, Zhang *et al* 2008, Tritscher *et al* 2011) suggested that the driving mechanisms for the soot restructuring are capillary forces, or other processes such as electrostatic forces, when water fills cavities (active sites) on the soot particle during condensation. However, other studies found that capillary forces lead to soot restucturing during evaporation of water instead of condensation (Ebert *et al* 2002, Zuberi *et al* 2005, Ma *et al* 2013). The degree of compaction might depend on the source of soot; for example, nascent diesel soot exhibited much smaller degree of compaction compared to soot produced from spark discharges between two graphite electrodes (Weingartner *et al* 1997).

In contrast, fewer studies have investigated soot processing by cold clouds and a mechanicistic understanding of the soot processing through ice cloud remains poor. The formation of porous structures after simulated cold cloud processing was observed in a past study for organic aerosols (Adler *et al* 2013). However, soot processing through ice cloud is still ellusive. Ice crystals can sublimate at the bottom edge of cirrus clouds or in the outflow of high convective clouds (Heymsfield *et al* 2010, Jensen *et al* 2011, Protat *et al* 2011). After sublimation, soot residuals can facilitate subsequent ice nucleation events by lowering the supersaturation threshold (preactivation effect) (Hobbs 1974, Knopf and Koop 2006). Additionally, soot residuals can fragment into smaller pieces or aggregate into larger soot clusters (Kärcher *et al* 2007). Petzold *et al* (1998) and Targino *et al* (2006) found soot particles in ice crystal residuals sampled from contrails and cirrus clouds, but did not study morphological features of the processed soot particles and the resulting changes in optical properties.

Here we investigate the changes in soot's morphology through cold cloud processing (supercooled droplet and ice crystal formation) and assess the effects of morphological changes on the optical properties of soot particles. We simulated the atmopheric condensation-drying and freeze-drying cloud cycles in a set of labolatory experiments during the soot aerosol aging study (SAAS) that was conducted at Pacific Northwest National Laboratory (PNNL). We experimentally determined the morphological properties of soot residuals from supercooled droplets and ice crystals, and modeled the optical properties of nascent and processed soot particles.

## 2. Experimental methods

### 2.1. Soot generation and characterization

The experiments were conducted in the environmental chamber facility at PNNL as part of SAAS in November of 2013 and January of 2014. Supplementary figure S1 shows the schematic of the experimental

setup. Soot particles were generated using a diesel generator (Pramac P6000S-4810) under a 5000 W load using a load bank (Simplex, Swift-E). The soot particles were then extracted from the generator exhaust and diluted with pure air by a factor of 10–11 at 130 °C using a heated venturi pump before cooling to room temperate. Co-emitted species, such as volatile organic carbon components and $NO_x$, were partially removed using a charcoal denuder. Soot particles were size selected (120 nm diameter) (supplementary figure S2) according to their electrical mobility with a differential mobility analyzer (DMA, TSI, 3081). Mobility size selected soot particles (figure S2) were injected (8600 $cm^{-3}$) into the environmental chamber.

A single particle mass spectrometer, SPLAT II (Zelenyuk *et al* 2009), was used for detailed real-time characterization of soot particles generated by the diesel engine. Particle characterization included measurements of mass, vacuum aerodynamic diameter (supplementary figure S2), and composition of individual particles sampled directly from the exhaust after mass or mobility classification. These data were used to determine particle effective density, material density, mass–mobility exponent, dynamic shape factors in free molecular and transition flow regimes, average diameter of monomers, number of monomers, and void fraction of soot agglomerates as described in details in a separate publication (Zelenyuk *et al* 2014).

### 2.2. Collection of residuals from supercooled droplets and ice crystals

Ice nucleation measurements of nascent soot particles were performed using a compact ice chamber (CIC) (Friedman *et al* 2011). Briefly, the CIC consists of two vertical independent temperature controlled parallel plates that are coated with an ice layer ~0.5 mm thick to produce ice-supersaturated humidity conditions inside the ice chamber. The evaporation section of the CIC, again coated with an ice layer ~0.5 mm thick, was maintained at a target temperature (−20 °C or −40 °C). The sheath and sample flow rates were 10 and 1 LPM, respectively, which led to an aerosol residence time of ~12 s within the chamber. The temperature gradient between the vertical plates was adjusted such that using Murphy and Koop (2005) vapor pressure formulations, the desired conditions of relative humidity with respect to water ($RH_w$) were obtained at a given fixed temperature. We performed laboratory experiments at two temperatures: −20 and −40 °C and at each temperature the $RH_w$ in the CIC was set to ~108 ± 3%. These humidity conditions generated supercooled droplets. At −20 °C we did not observe ice crystals, while ice crystals were formed at −40 °C due to homogeneous freezing. We confirmed the absence of ice crystals and the presence of supercooled droplets at −20 °C by observing the size distribution of particles (supercooled droplets are in the range of 2.5–4.2 $\mu$m, while ice crystals are in the range of 6–9 $\mu$m in diameter) exiting the CIC using an optical particle counter (OPC; CLiMET, model CI-3100) (Kulkarni *et al* 2012, Kulkarni *et al* 2015). These results are in agreement with previous work where particles generated by miniCAST soot generator were used (Friedman *et al* 2011). Ice crystals and supercooled droplets were seperated from the interstitial particles using a pumped counterflow virtual impactor (PCVI) (Kulkarni *et al* 2011) and passed through a diffusion dryer to collect the dry residuals. The 50% cut-off size of PCVI was set to transmit droplets and ice particles larger than ~4 $\mu$m. The residuals of the transmitted cloud hydrometeors were impacted on substrates for electron microscopy analysis using a four-stage cascade impactor (MPS-4G1). The samples analyzed here were collected on the fourth stage with a 50% cut-off aerodynamic diameters of 50 nm. Soot particles were collected on 300 mesh transmission electron microscopy (TEM) copper lacey formvar grids (Ted Pella, Inc.). As a reference, nascent soot particles were also collected directly from the environmental chamber, before entering into the CIC. Nascent soot particles were also collected on nucleopre polycarbonate membranes using a custom built aspirated sampler for scanning electron microscopy (SEM) analysis.

### 2.3. Morphological characterization

Individual nascent soot particles, and residuals from ice crystals and supercooled droplets were investigated using a field-emission SEM (Hitachi S-4700) and a TEM (JEOL JEM-2010). Freshly emitted soot particles are often represented as fractal-like aggregates due to their self-similar structures over several length scales (Oh and Sorensen 1997) and can be described by the following scaling law.

$$N = k_g \left( \frac{2R_g}{d_p} \right)^{D_f}, \quad (1)$$

where $N$ is the number of monomers per aggregate, $D_f$ is the mass fractal dimension, $R_g$ is the radius of gyration, $d_p$ is the monomer diameter, $k_g$ is the fractal proportionality constant or fractal prefactor. We used the ensemble method to calculate the 3D fractal dimension of nascent soot particles from 2D images (Brasil *et al* 1999, Chakrabarty *et al* 2006, China *et al* 2014). However, soot particles from supercooled and ice crystal residuals were very compact (see section 3.1), presumably resulting in a $D_f > 2$. In this limit, $N$ would be underestimated due to the significant overlap of the monomers in the 2D image. Therefore, instead of using equation (1), we calculated a 2D fractal dimension ($D_{2f}$ such that for a sphere $D_{2f}$ would be equal to 2) using the directly measurable area of each aggregate ($A_a$) and its maximum length ($L_{max}$) (Lee and Kramer 2004) using the following scaling law (China *et al* 2015):

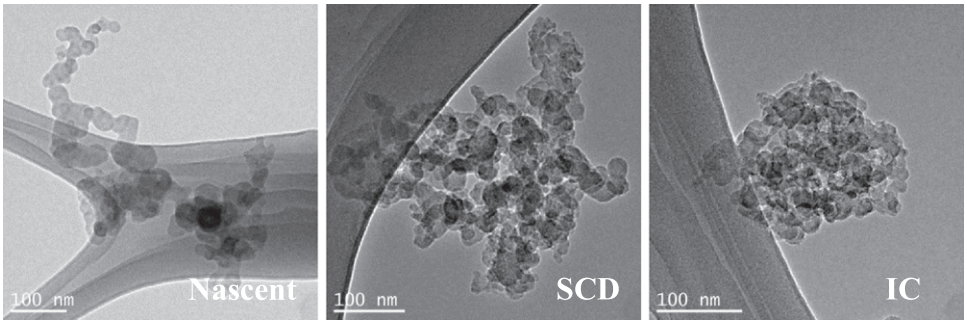


**Figure 1.** Examples of TEM images of nascent soot (left panel), supercooled droplet (SCD) residuals (middle panel) and ice crystal (IC) residuals (right panel).

$$A_a = k_{2g}\left(L_{\max}\right)^{D_{2f}} \quad (2)$$

For direct comparison purpose, we calculated $D_{2f}$ for nascent soot particles as well (supplementary figure S3). We also used several other 2D morphological descriptors such as projected area equivalent diameter ($D_{\mathrm{Aeq}}$), aspect ratio, roundness and convexity to characterize nascent soot, and supercooled droplet and ice crystal residuals. The $D_{\mathrm{Aeq}}$ is defined as the diameter of a spherical particle of the same projected area. The aspect ratio represents the level of elongation of the particle defined as the ratio of the longest dimension ($L_{\max}$) to the orthogonal width ($W_{\max}$). Roundness is the ratio of the projected area of the particle ($A_p$) to the area of a circle with $L_{\max}$ as the diameter. Higher roundness indicates particles that are more compact. The convexity is defined as the ratio of $A_p$ and the area of the convex hull polygon (smallest convex polygon in which the particle is inscribed). In this study, we assessed the morphological characteristics of 200–240 individual particles for each samples. A detailed description of the image processing and the analysis of the morphological parameters and their limitations is provided elsewhere (China *et al* 2013, China *et al* 2014).

### 2.4. Simulation of optical properties

We investigated the effect of compaction on the optical properties of soot particles as a function of wavelength, using the discrete dipole approximation (DDA-DDSCAT7.3) code (Draine and Flatau 1994, 2013). In particular in this study, we discuss parameters relevant to radiative forcing calculations, including the absorption ($C_{\mathrm{abs}}$) and scattering cross-sections ($C_{\mathrm{sca}}$), the single scattering albedo (SSA $= C_{\mathrm{sca}}/(C_{\mathrm{abs}} + C_{\mathrm{sca}})$), and the asymmetry parameter ($g$). We used a random walk aggregation method to generate model soot particles for the DDA simulations (Richard *et al* 2011). The detailed method for the generation of the aggregates and for the DDA simulations are described elsewhere (Scarnato *et al* 2013). We modeled soot aggregates with 100 monomers with a diameter of 23 nm, in agreement with our observed mean values for nascent soot from electron microscopy and the measurements by SPLAT II, ice crystal and supercooled droplet residuals (see sections 3.1 and 3.2). We report the morphological parameters of the modeled soot aggregates representing nascent soot, supercooled droplet residuals, and ice crystal residuals in the supplementary table S1. We computed values of scattering and absorption cross sections averaged over 1000 random particle orientations (see Scarnato *et al* (2013) for discussion on the solution convergence due to the average of number of orientations). We performed the calculations at four different wavelengths of 450, 532, 781 and 550 nm; the first three corresponding to wavelengths used by several laser-based instruments for aerosol optical characterization and the last one to allow for a direct comparison with data available in literature that are often reported at 550 nm. We used the soot refractive index provided by Chang and Charalampopoulos (1990) for all the calculations (Scarnato *et al* 2015).

## 3. Results and discussions

### 3.1. Nascent soot characterization

The composition analysis by SPLAT II revealed that soot particles generated by this diesel engine were composed of 80% elemental carbon, 5% oxygenated organics, and 15% PAHs, yielding an estimate for soot material density of 1.9 g cm$^{-3}$. Furthermore, the measurements on the mass- and mobility-selected particles indicate, for example, that nascent soot particles with mobility diameter of 120 nm had mass of 0.56 fg, volume equivalent diameter of 83 nm, void fraction of 0.67, and were comprised on average of 67 monomers with diameter of 22 nm.

### 3.2. Morphology of residuals

We begin by comparing the morphologies of soot residuals from supercooled water droplets and ice crystals with the morphology of nascent soot particles. In figure 1 we show examples of TEM images of individual nascent soot particles, and soot residuals from supercooled droplets and ice crystals. The open fractal-like structure of nascent soot particles

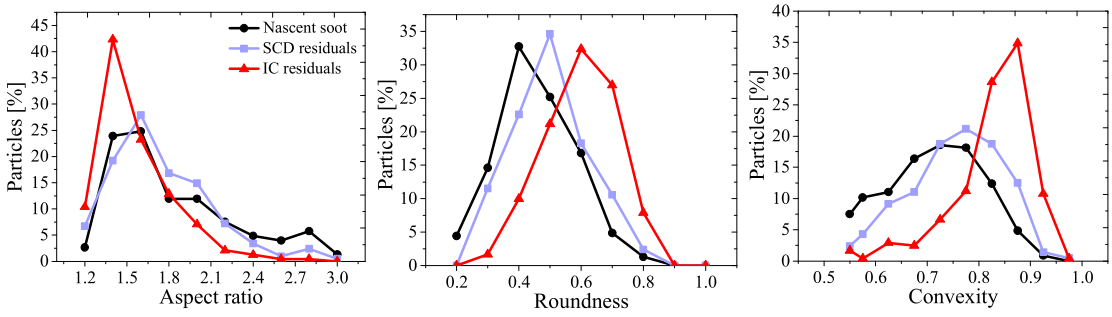


**Figure 2.** Distributions of aspect ratio (left panel), roundness (middle panel) and convexity (right panel) for nascent soot (black), soot from supercooled droplet (SCD) residuals (light blue) and ice crystal (IC) residuals (red). Number of particles analyzed for nascent soot, supercooled and ice crystal residuals were 226, 208 and 241, respectively.

**Table 1.** Mean values of several morphological descriptors for: (a) nascent soot, (b) soot from supercooled droplet residuals, and (c) soot from ice crystal residuals.

| Samples | $n$ | $d_p$ (nm) | $D_{Aeq}$ (nm) | AR | RN | CV | $D_{2f}$ | $k_{2g}$ |
|---|---|---|---|---|---|---|---|---|
| Nascent soot | 226 | 23(3) | 153(45) | 1.75(0.48) | 0.41(0.12) | 0.71(0.10) | 1.42(0.05) | 0.13(0.03) |
| SCD residuals | 208 | 23(5) | 179(75) | 1.65(0.37) | 0.45(0.12) | 0.75(0.10) | 1.61(0.03) | 0.20(0.02) |
| IC residuals | 241 | 24(4) | 201(61) | 1.46(0.27) | 0.55(0.11) | 0.83(0.08) | 1.71(0.04) | 0.28(0.02) |

Note: $n$—number of individual particles analyzed; $d_p$—monomer diameter; $D_{Aeq}$—projected area equivalent diameter; AR—aspect ratio; RN—roundness; CV—convexity; $D_{2f}$—2D fractal dimension; $k_{2g}$—2D prefactor. In parenthesis—standard error for $D_{2f}$ and $k_{2g}$ (calculated from the uncertainty in the mean-square fit), and standard deviation for the other parameters.

exhibited a $D_f$ of 1.53 $\pm$ 0.02 and a $k_g$ of 3.44 $\pm$ 0.06. For diesel soot, previous studies showed $D_f$ values ranging between 1.20 and 1.82 depending on engine conditions and combustion properties (e.g., Luo *et al* 2005, Li *et al* 2011). The center and right panels in figure 1 show the morphology of supercooled droplet residuals and ice crystal residuals, respectively. The residuals appear to be more compact than nascent soot.

Figure 2 compares the distribution of aspect ratio (left panel), roundness (middle panel) and convexity (right panel) for nascent soot, soot from supercooled droplet residuals and soot from ice crystal residuals, respectively. Soot particles from ice crystal residuals are the most compact (higher roundness and convexity, and lower aspect ratio) followed by supercooled droplet residuals and nascent soot particles. On average, soot from ice crystal residuals is more compact than supercooled droplet residuals as indicated by the respective ~34% and ~10% increases in roundness compared to nascent soot), suggesting that the freezing process results in more extensive restructuring of soot. A consistent pattern is seen also from the 2D fractal dimension (table 1); $D_{2f}$ is highest for soot from ice crystal residuals, followed by soot from supercooled droplet residuals, and finally, by nascent soot. Higher $D_{2f}$ also represents more compact structures.

These observarions of morphological changes of soot particles are in accord with the measurements conducted by SPLAT II on soot particles coated with secondary organic aerosol (SOA). In a separate set of the SAAS experiments it was shown that fractal-like nascent soot particles become compacted after coating and subsequent thermal removal of SOA coating. As a result, the effective density of soot particles increases from 0.58 g cm$^{-3}$ for uncoated fractal nascent soot particles to 0.96 g cm$^{-3}$ for the compact soot.

Table 1 summarizes the mean and standard deviation values for selected morphological descriptors (aspect ratio, roundness and convexity) including 2D fractal dimension and prefactor. Mean values of $D_{Aeq}$ in table 1 show that soot particles from the ice crystal residuals (201 nm) exhibited the largest sizes followed by soot from supercooled residuals (179 nm) and nascent soot particles (153 nm). This is also consistent with their size distribution (supplementary figure S4). Coagulation of soot before entering the CIC can be responsible for the overall larger size of soot from supercooled droplet and ice crystal residuals. In addition, we suspect that some interstitial particles along with the desired size supercooled water droplets and ice crystals may have been transmitted through the PCVI (Pekour and Cziczo 2011).

### 3.3. Compaction of soot particles

Some degree of compaction (roundness ~0.45) of soot residuals from the supercooled droplets can occur either during droplet condensation on soot particles due to surface tension (Kutz and Schmidt-Ott 1992) and capillary forces (Tritscher *et al* 2011) or during evaporation (Ma *et al* 2013). We observed that ice crystal residuals were more compact (roundness ~0.55) than supercooled droplet residuals, suggesting

that the atmospheric freeze-drying process perhaps playing a role in further restructuring of the soot particles. Expansion of water during freezing leads to presure developement inside the droplet and stresses in the shell of the frozen droplet, resulting in the growth of spikes or bulges (deformation of the shell) on the frozen droplet surface and even shattering of the shell if sufficient elastic energy is stored (Hobbs and Alkezweeny 1968, Johnson and Hallett 1968, King and Fletcher 1973, López and Ávila 2012). The pressure that develops inside the droplet and can be in the order of ~7600 kPa for 7 mm droplets (Visagie 1969) and ~8900 kPa for 10 mm droplets (King and Fletcher 1973). The magnitude of the pressure depends on the parameters such as droplet size, temperature, total freezing time and visco-elastic properties of ice (see discussion in supplementary material figures S5 and S6). The pressure inside the droplet increases with freezing time and it is higher for colder freezing temperatures (King and Fletcher 1973). The mechanical stress during freezing can alter the shape of the soot particle and the magnitude of the soot–water contact angle and filling angle (Butt and Kappl 2009), resulting in changes of the capilary force (Rahman 2001) and finally leading to the compaction of the soot structure. Previous studies suggested that the developement of surface stresses and compression forces during freezing process results in deformed shapes of biological material (Zhang *et al* 2006), wooden fibers (Macfarlane *et al* 2012) and materials used in pharmaceutical science (Zijlstra *et al* 2004). We suggest that similar stresses and compression are reponsible for the compaction of soot particles that we observed during the atmospheric freeze-drying process. The drying process (that occurs within the flow line between PCVI and cascade impactor; see section 2.2) can also contribute to the compaction of soot particles. We believe that both freezing and drying processes lead to higher compaction of the soot particles.

### 3.4. Optical properties of residuals

The optical properties of single nascent soot particles, as well as soot particles from supercooled droplet residuals and ice crystal residuals were simulated using the DDA model described earlier (supplementary table S2). Figure 3 shows the spectral dependence of several optical properties, including absorption ($C_{abs}$) and scattering ($C_{sca}$) cross-sections, SSA and asymmetry parameter ($g$) of soot residuals from supercooled droplets and ice crystals, normalized by the correspondent property of nascent soot. DDA predicts higher optical cross sections and SSA for compact aggregates. Soot residuals from ice crystals and supercooled droplets have a slightly higher $C_{abs}$ ($C_{abs\text{-IC residuals}}/C_{abs\text{-nascent}}$ is 1.05 and $C_{abs\text{-SCD residuals}}/C_{abs\text{-nascent}}$ is 1.03 at 550 nm) than nascent soot. However, soot residuals from ice crystals have substantially higher $C_{sca}$ ($C_{sca\text{-IC residuals}}/C_{sca\text{-nascent}}$ is 1.37 at 550 nm) than nascent soot. These results are consistent with an increase in modeled $C_{sca}$ for highly compact soot collected in the free troposphere in the North Atlantic (China *et al* 2015). Similarly, a previous T-matrix simulation study showed an increase in $C_{abs}$ and $C_{sca}$ at 870 nm for compact soot compared to less compact soot (Liu *et al* 2008). Less material is exposed to the light when soot particles are more compact, decreasing the absorption. At the same time, monomer-monomer interactions increase, resulting in an overall small enhancement (<10%) of absorption. Similarly, increase in monomer–monomer interactions results in higher scattering for compact soot (China *et al* 2015). Overall, our results show higher SSA for compact soot (IC residuals) than for lacey soot (nascent) and the SSA ratios ($SSA_{IC\ residuals}/SSA_{nascent}$) are 1.40, 1.30, 1.28 and 1.15 at 450, 532, 550 and 781 nm, respectively. These results are consistent with direct measurement of optical properties using photoacoustic and cavity ring-down spectroscopy by Radney *et al* (2014). They found that soot compaction increases SSA by a factor of ~1.2 at 405 nm for relatively smaller monomer diameter (17 nm) and smaller soot size (geometric mean mobility diameter of soot: 116.7 nm) compared to our study. However, future studies should focus on *in situ* measurements of the optical properties of supercoooled droplet residuals and ice crystal residuals simultaneously with the morphological characterization of the soot particles. Our DDA simulation results are also consistent with a previous simulation study (Kahnert and Devasthale 2011, Liu *et al* 2008) that used T-matrix. They also found an increase in SSA due to soot compaction and the magnitude of the difference in SSA depends on monomer diameter, number of monomers, refractive index of soot and wavelength. For example, Liu *et al* (2008) found that the SSA ratio ($SSA_{compact}/SSA_{lacey}$) increases from 4.25 to 5.25 as soot size increases (from $N = 200$ to $N = 400$) for a monomer diameter of 15 nm at 870 nm wavelength. Our previous study also shows higher SSA ratio (1.98 versus 1.66) for larger soot ($N = 150$) compared to relatively smaller soot size ($N = 66$) for a monomer diameter of 34 nm at 450 nm wavelength. Compact soot particles exhibit lower $g$ compared to open fractal-like nascent soot particles for visible wavelengths. In figure 3 we show that the normalized $g$ values (normalized by the $g$ value of nascent soot) are <1 for both ice crystal residuals and supecooled droplet with the first being the lowest. These results suggest an overall higher SSA and lower $g$ for compact soot particles with respect to nascent soot. Both SSA and $g$ are input parameters into radiative transfer models. A simple estimate of the top-of-the atmosphere direct radiative forcing (TOA-DRF) using the conceptual calculation (Chylek and Wong 1995,

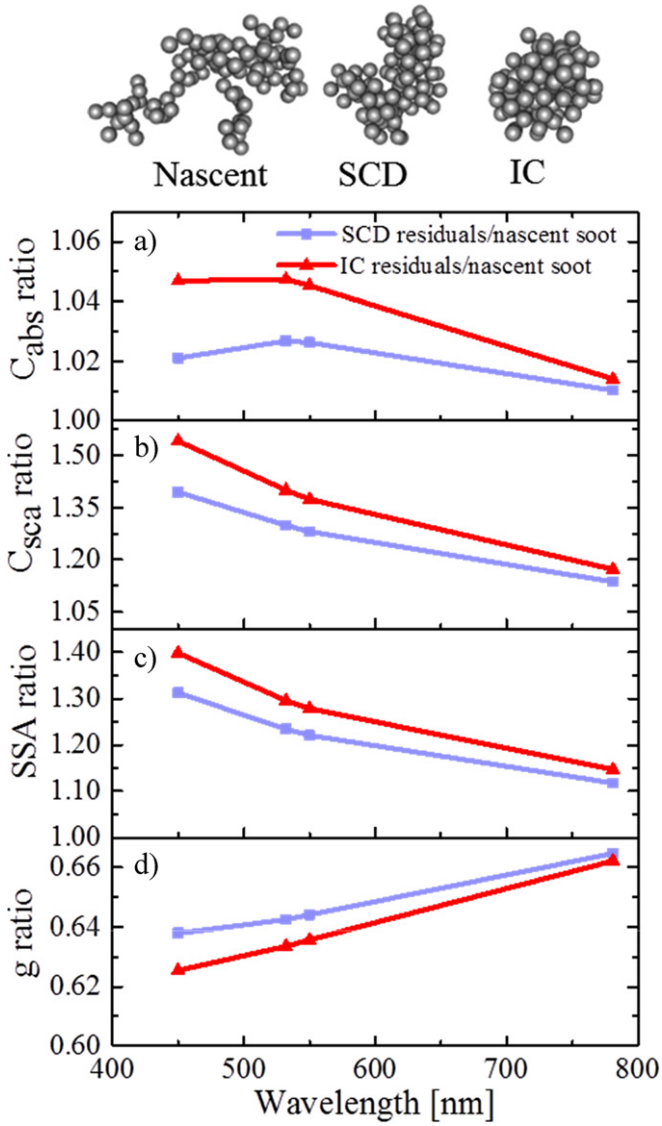


**Figure 3.** Images on top show the modeled soot particles used in the simulations, representing from left to right, open fractal-like nascent soot, soot residual from supercooled droplet (SCD) and ice crystal (IC). Normalized absorption (a) and scattering cross-sections (b), single scattering albedo (SSA) (c), and asymmetry parameter (*g*) (d), as functions of wavelength calculated using the discrete dipole approximation (DDA). The modeled soot particles were constructed by 100 monomers with 23 nm diameter each and different degrees of compaction to represent the measured morphological values. Optical cross-sections, SSA and *g* for SCD and IC soot residuals were normalized by the values obtained for nascent soot.

Haywood and Shine 1995, Lenoble *et al* 1982) shows that soot compaction due to atmospheric freeze-drying cycle typically results in a reduction of the positive soot TOA-DRF and the degree of reduction depends on the wavelength and surface albedo (supplementary figure S7). A maximum reduction of 63% in TOA-DRF ([TOA-$DRF_{IC\ residual}$-TOA-$DRF_{Nascent}$]/TOA-$DRF_{IC\ residual}$) is estimated for ice crystal residuals, while a maximum 45% reduction is estimated for supercooled droplet residuals due to compaction. Similarly, Kahnert and Devasthale (2011) found trends of reduction (up to 60%) of TOA-DRF for compact soot compared to lacey soot. Future studies should also focus on rigorous radiative forcing calculations by incorporating residual soot concentration, size distribution and other size dependent parameters.

## 4. Summary and conclusions

We performed a set of laboratory experiments to simulate atmospheric cold cloud processing of soot particles by analyzing individual dry residual soot particles from supercooled droplets and ice crystals. We found that soot particles from ice crystal residuals experienced higher compaction compared to supercooled droplet residuals. These results suggest that the atmospheric freeze-drying cycle is perhaps more effective at compacting soot than the condensation-drying cycle. We performed numerical simulations of soot optical properties, guided by quantitative assessment of the morphology of nascent soot and soot from supercooled droplet and ice crystal residuals. Simulated compact soot residuals from ice crystals

displayed higher SSA than soot residuals from supercooled droplets and nascent soot particles of the same mass. Compaction of soot particles through cold clouds processing can alter their lifetime, global burden (Van Poppel *et al* 2005), and radiative forcing (Van Poppel *et al* 2005, Kahnert and Devasthale 2011, Mishchenko *et al* 2014, China *et al* 2015). These results could have significant implications on our understanding of the microphysical and optical properties of soot in cirrus and contrails. Future studies should focus on elucidating how cold cloud processing of soot particles internally mixed with organics and sulfate alter their morphology and optical properties. Additionally, further effort should be made to develop a microphysical-based parameterization of soot compaction to be used in climate models.

## Acknowledgments

This work was funded by the US Department of Energy's Atmospheric System Research (grant no DE-SC0010019), the US National Science Foundation grant (grant no AGS-1119164) and the Research Initiation Grant from Department of Defense. S China and C Mazzoleni acknowledge a NASA Earth and Space Science Graduate Fellowship (grant no NNX13AN68H). We thank Owen P Mills for helping with the TEM work. BS would like to acknowledge Denis Richard for providing the aggregation code. MD, AA and SL acknowledge support by US DOE Office of Biological and Environmental Research, Atmospheric System Research Program, F265 to LANL. GK, MP, JS, JW, AZ, DC, AL and RZ acknowledge support by US DOE Office of Biological and Environmental Research (OBER), Atmospheric System Research Program. Support was also provided by the Environmental Molecular Sciences Laboratory (EMSL), a national scientific user facility sponsored by the DOE's OBER at Pacific Northwest National Laboratory (PNNL). PNNL is operated for DOE by Battelle Memorial Institute under contract DE-AC05-76RL01830.

## References

Adler G, Koop T, Haspel C, Taraniuk I, Moise T, Koren I, Heiblum R H and Rudich Y 2013 Formation of highly porous aerosol particles by atmospheric freeze-drying in ice clouds *Proc. Natl Acad. Sci. USA* **110** 20414–9

Bond T C *et al* 2013 Bounding the role of black carbon in the climate system: a scientific assessment *J. Geophys. Res.—Atmos.* **118** 5380–552

Brasil A M, Farias T L and Carvalho M G 1999 A recipe for image characterization of fractal-like aggregates *J. Aerosol Sci.* **30** 1379–89

Butt H-J and Kappl M 2009 Normal capillary forces *Adv. Colloid Interface Sci.* **146** 48–60

Chakrabarty R K, Moosmüller H, Garro M A, Arnott W P, Walker J, Susott R A, Babbitt R E, Wold C E, Lincoln E N and Hao W M 2006 Emissions from the laboratory combustion of wildland fuels: particle morphology and size *J. Geophys. Res.—Atmos.* **111** D07204

Chang H and Charalampopoulos T 1990 Determination of the wavelength dependence of refractive indices of flame soot *Proc. R. Soc.* A **430** 577–91

China S, Mazzoleni C, Gorkowski K, Aiken A C and Dubey M K 2013 Morphology and mixing state of individual freshly emitted wildfire carbonaceous particles *Nat. Commun.* **4** 2122

China S, Salvadori N and Mazzoleni C 2014 Effect of traffic and driving characteristics on morphology of atmospheric soot particles at freeway on-ramps *Environ. Sci. Technol.* **48** 3128–35

China S *et al* 2015 Morphology and mixing state of aged soot particles at a remote marine free troposphere site: implications for optical properties *Geophys. Res. Lett.* **42** 2014GL062404

Chylek P and Wong J 1995 Effect of absorbing aerosols on global radiation budget *Geophys. Res. Lett.* **22** 929–31

Colbeck I, Appleby L, Hardman E and Harrison R M 1990 The optical properties and morphology of cloud-processed carbonaceous smoke *J. Aerosol Sci.* **21** 527–38

Crawford I *et al* 2011 Studies of propane flame soot acting as heterogeneous ice nuclei in conjunction with single particle soot photometer measurements *Atmos. Chem. Phys.* **11** 9549–61

Cziczo D J and Froyd K D 2014 Sampling the composition of cirrus ice residuals *Atmos. Res.* **142** 15–31

Cziczo D J, Froyd K D, Hoose C, Jensen E J, Diao M, Zondlo M A, Smith J B, Twohy C H and Murphy D M 2013 Clarifying the dominant sources and mechanisms of cirrus cloud formation *Science* **340** 1320–4

Demott P J 1990 An exploratory-study of ice nucleation by soot aerosols *J. Appl. Meteorol.* **29** 1072–9

DeMott P J, Chen Y, Kreidenweis S M, Rogers D C and Sherman D E 1999 Ice formation by black carbon particles *Geophys. Res. Lett.* **26** 2429–32

Diehl K and Mitra S K 1998 A laboratory study of the effects of a kerosene-burner exhaust on ice nucleation and the evaporation rate of ice crystals *Atmos. Environ.* **32** 3145–51

Draine B T and Flatau P J 1994 Discrete-dipole approximation for scattering calculations *J. Opt. Soc. Am.* A **11** 1491–9

Draine B T and Flatau P J 2013 User guide for the discrete dipole approximation code DDSCAT 7.3 (arXiv: 1305.6497)

DyMarska M, Murray B J, Sun L, Eastwood M L, Knopf D A and Bertram A K 2006 Deposition ice nucleation on soot at temperatures relevant for the lower troposphere *J. Geophys. Res.—Atmos.* **111** D04204

Ebert M, Inerle-Hof M and Weinbruch S 2002 Environmental scanning electron microscopy as a new technique to determine the hygroscopic behaviour of individual aerosol particles *Atmos. Environ.* **36** 5909–16

Ellis A *et al* 2015 Characterizing black carbon in rain and ice cores using coupled tangential flow filtration and transmission electron microscopy *Atmos. Meas. Tech. Discuss.* **8** 6015–43

Fornea A P, Brooks S D, Dooley J B and Saha A 2009 Heterogeneous freezing of ice on atmospheric aerosols containing ash, soot, and soil *J. Geophys. Res.—Atmos.* **114** D13201

Friedman B, Kulkarni G, Beránek J, Zelenyuk A, Thornton J A and Cziczo D J 2011 Ice nucleation and droplet formation by bare and coated soot particles *J. Geophys. Res.—Atmos.* **116** D17203

Gorbunov B, Baklanov A, Kakutkina N, Windsor H L and Toumi R 2001 Ice nucleation on soot particles *J. Aerosol Sci.* **32** 199–215

Hansen J and Nazarenko L 2004 Soot climate forcing via snow and ice albedos *Proc. Natl Acad. Sci. USA* **101** 423–8

Hansson H C and Ahlberg M S 1985 Dynamic shape factors of sphere aggregates in an electric-field and their dependence on the Knudsen number *J. Aerosol Sci.* **16** 69–79

Haywood J M and Shine K P 1995 The effect of anthropogenic sulfate and soot aerosol on the clear sky planetary radiation budget *Geophys. Res. Lett.* **22** 603–6

Heymsfield A, Baumgardner D, DeMott P, Forster P, Gierens K and Kärcher B 2010 Contrail Microphysics *Bull. Am. Meteorol. Soc.* **91** 465–72

Hobbs P V 1974 *Ice Physics* vol 1 (Oxford: Clarendon) p 837

Hobbs P V and Alkezweeny A J 1968 The fragmentation of freezing water droplets in free fall *J. Atmos. Sci.* **25** 881–8

Hoose C and Möhler O 2012 Heterogeneous ice nucleation on atmospheric aerosols: a review of results from laboratory experiments *Atmos. Chem. Phys. Discuss.* **12** 12531–621

Huang P-F, Turpin B J, Pipho M J, Kittelson D B and McMurry P H 1994 Effects of water condensation and evaporation on diesel chain-agglomerate morphology *J. Aerosol Sci.* **25** 447–59

Jacobson M Z 2006 Effects of externally-through-internally-mixed soot inclusions within clouds and precipitation on global climate *J. Phys. Chem.* A **110** 6860–73

Jensen E, Pfister L and Toon O 2011 Impact of radiative heating, wind shear, temperature variability, and microphysical processes on the structure and evolution of thin cirrus in the tropical tropopause layer *J. Geophys. Res.—Atmos.* **116** D12209

Johnson D A and Hallett J 1968 Freezing and shattering of supercooled water drops *Q. J. R. Meteorol. Soc.* **94** 468–82

Kahnert M and Devasthale A 2011 Black carbon fractal morphology and short-wave radiative impact: a modelling study *Atmos. Chem. Phys.* **11** 11745–59

Kärcher B, Busen R, Petzold A, Schröder F P, Schumann U and Jensen E J 1998 Physicochemistry of aircraft-generated liquid aerosols, soot, and ice particles: II. Comparison with observations and sensitivity studies *J. Geophys. Res.—Atmos.* **103** 17129–47

Kärcher B, Möhler O, DeMott P J, Pechtl S and Yu F 2007 Insights into the role of soot aerosols in cirrus cloud formation *Atmos. Chem. Phys.* **7** 4203–27

Khalizov A F, Lin Y, Qiu C, Guo S, Collins D and Zhang R 2013 Role of OH-initiated oxidation of isoprene in aging of combustion soot *Environ. Sci. Technol.* **47** 2254–63

King W and Fletcher N 1973 Pressures and stresses in freezing water drops *J. Phys. D: Appl. Phys.* **6** 2157

Knopf D A and Koop T 2006 Heterogeneous nucleation of ice on surrogates of mineral dust *J. Geophys. Res.—Atmos.* **111** D12201

Kulkarni G, Fan J, Comstock J M, Liu X and Ovchinnikov M 2012 Laboratory measurements and model sensitivity studies of dust deposition ice nucleation *Atmos. Chem. Phys.* **12** 7295–308

Kulkarni G, Nandasiri M, Zelenyuk A, Beranek J, Madaan N, Devaraj A, Shutthanandan V, Thevuthasan S and Varga T 2015 Effects of crystallographic properties on the ice nucleation properties of volcanic ash particles *Geophys. Res. Lett.* **42** 2015GL063270

Kulkarni G, Pekour M, Afchine A, Murphy D M and Cziczo D J 2011 Comparison of experimental and numerical studies of the performance characteristics of a pumped counterflow virtual impactor *Aerosol Sci. Technol.* **45** 382–92

Kutz S and Schmidt-Ott A 1992 Characterization of agglomerates by condensation-induced restructuring *J. Aerosol Sci.* **23** 357–60

Lee C and Kramer T A 2004 Prediction of three-dimensional fractal dimensions using the two-dimensional properties of fractal aggregates *Adv. Colloid Interface Sci.* **112** 49–57

Lenoble J, Tanre D, Deschamps P Y and Herman M 1982 A simple method to compute the change in earth-atmosphere radiative balance due to a stratospheric aerosol layer *J. Atmos. Sci.* **39** 2565–76

Lewis K, Arnott W, Moosmüller H, Chakrabarty R, Carrico C, Kreidenweis S, Day D, Malm W, Laskin A and Jimenez J 2009 Reduction in biomass burning aerosol light absorption upon humidification: roles of inorganically-induced hygroscopicity, particle collapse, and photoacoustic heat and mass transfer *Atmos. Chem. Phys.* **9** 8949–66

Li Z, Song C, Song J, Lv G, Dong S and Zhao Z 2011 Evolution of the nanostructure, fractal dimension and size of in-cylinder soot during diesel combustion process *Combust. Flame* **158** 1624–30

Liu L, Mishchenko M I and Arnott W P 2008 A study of radiative properties of fractal soot aggregates using the superposition T-matrix method *J. Quant. Spectrosc. Radiat. Transfer* **109** 2656–63

Lohmann U and Feichter J 2005 Global indirect aerosol effects: a review *Atmos. Chem. Phys.* **5** 715–37

López M L and Ávila E E 2012 Deformations of frozen droplets formed at −40 °C *Geophys. Res. Lett.* **39** L01805

Luo C-H, Grace Lee W-M, Lai Y-C, Wen C-Y and Liaw J-J 2005 Measuring the fractal dimension of diesel soot agglomerates by fractional Brownian motion processor *Atmos. Environ.* **39** 3565–72

Ma X, Zangmeister C D, Gigault J, Mulholland G W and Zachariah M R 2013 Soot aggregate restructuring during water processing *J. Aerosol Sci.* **66** 209–19

Macfarlane A L, Kadla J F and Kerekes R J 2012 High performance air filters produced from freeze-dried fibrillated wood pulp: fiber network compression due to the freezing process *Ind. Eng. Chem. Res.* **51** 10702–11

Mikhailov E, Vlasenko S, Podgorny I, Ramanathan V and Corrigan C 2006 Optical properties of soot–water drop agglomerates: an experimental study *J. Geophys. Res.—Atmos.* **111** D07209

Mishchenko M I, Liu L, Cairns B and Mackowski D W 2014 Optics of water cloud droplets mixed with black-carbon aerosols *Opt. Lett.* **39** 2607–10

Möhler O, Linke C, Saathoff H, Schnaiter M, Wagner R, Mangold A, Krämer M and Schurath U 2005 Ice nucleation on flame soot aerosol of different organic carbon content *Meteorol. Z.* **14** 477–84

Murphy D and Koop T 2005 Review of the vapour pressures of ice and supercooled water for atmospheric applications *Q. J. R. Meteorol. Soc.* **131** 1539–65

Oh C and Sorensen C M 1997 The effect of overlap between monomers on the determination of fractal cluster morphology *J. Colloid Interface Sci.* **193** 17–25

Pekour M S and Cziczo D J 2011 Wake capture, particle breakup, and other artifacts associated with counterflow virtual impaction *Aerosol Sci. Technol.* **45** 758–64

Persiantseva N M, Popovicheva O B and Shonija N K 2004 Wetting and hydration of insoluble soot particles in the upper troposphere *J. Environ. Monit.* **6** 939–45

Petzold A, Döpelheuer A, Brock C A and Schröder F 1999 *In situ* observations and model calculations of black carbon emission by aircraft at cruise altitude *J. Geophys. Res.—Atmos.* **104** 22171–81

Petzold A, Ström J, Ohlsson S and Schröder F P 1998 Elemental composition and morphology of ice-crystal residual particles in cirrus clouds and contrails *Atmos. Res.* **49** 21–34

Protat A, Delanoë J, May P, Haynes J, Jakob C, O'connor E, Pope M and Wheeler M 2011 The variability of tropical ice cloud properties as a function of the large-scale context from ground-based radar-lidar observations over Darwin, Australia *Atmos. Chem. Phys.* **11** 8363–84

Radney J G, You R, Ma X, Conny J M, Zachariah M R, Hodges J T and Zangmeister C D 2014 Dependence of soot optical properties on particle morphology: measurements and model comparisons *Environ. Sci. Technol.* **48** 3169–76

Rahman M S 2001 Toward prediction of porosity in foods during drying: a brief review *Drying Technol.* **19** 1–13

Ramanathan V and Carmichael G 2008 Global and regional climate changes due to black carbon *Nat. Geosci.* **1** 221–7

Richard D, Glenar D, Stubbs T, Davis S and Colaprete A 2011 Light scattering by complex particles in the Moon's exosphere: toward a taxonomy of models for the realistic simulation of the scattering behavior of lunar dust *Planet. Space Sci.* **59** 1804–14

Scarnato B V, China S, Nielsen K and Mazzoleni C 2015 Perturbations of the optical properties of mineral dust particles by mixing with black carbon: a numerical simulation study *Atmos. Chem. Phys.* **15** 6913–28

Scarnato B V, Vahidinia S, Richard D T and Kirchstetter T W 2013 Effects of internal mixing and aggregate morphology on

optical properties of black carbon using a discrete dipole approximation model *Atmos. Chem. Phys.* **13** 5089–101

Schumann U, Jeßberger P and Voigt C 2013 Contrail ice particles in aircraft wakes and their climatic importance *Geophys. Res. Lett.* **40** 2867–72

Storelvmo T 2012 Uncertainties in aerosol direct and indirect effects attributed to uncertainties in convective transport parameterizations *Atmos. Res.* **118** 357–69

Streets D G, Bond T C, Lee T and Jang C 2004 On the future of carbonaceous aerosol emissions *J. Geophys. Res.—Atmos.* **109** D24212

Targino A C, Krejci R, Noone K J and Glantz P 2006 Single particle analysis of ice crystal residuals observed in orographic wave clouds over Scandinavia during INTACC experiment *Atmos. Chem. Phys.* **6** 1977–90

Tritscher T, Jurányi Z, Martin M, Chirico R, Gysel M, Heringa M F, DeCarlo P F, Sierau B, Prévôt A S and Weingartner E 2011 Changes of hygroscopicity and morphology during ageing of diesel soot *Environ. Res. Lett.* **6** 034026

Twohy C H and Poellot M R 2005 Chemical characteristics of ice residual nuclei in anvil cirrus clouds: evidence for homogeneous and heterogeneous ice formation *Atmos. Chem. Phys.* **5** 2289–97

Van Poppel L H, Friedrich H, Spinsby J, Chung S H, Seinfeld J H and Buseck P R 2005 Electron tomography of nanoparticle clusters: implications for atmospheric lifetimes and radiative forcing of soot *Geophys. Res. Lett.* **32** L24811

Visagie P 1969 Pressures inside freezing water drops *J. Glaciol.* **8** 301–9

Wang H 2011 Formation of nascent soot and other condensed-phase materials in flames *Proc. Combust. Inst.* **33** 41–67

Weingartner E, Burtscher H and Baltensperger U 1997 Hygroscopic properties of carbon and diesel soot particles *Atmos. Environ.* **31** 2311–27

Zelenyuk A, Yang J, Choi E and Imre D 2009 SPLAT: II. An aircraft compatible, ultra-sensitive, high precision instrument for *in situ* characterization of the size and composition of fine and ultrafine particles *Aerosol Sci. Technol.* **43** 411–24

Zelenyuk A *et al* 2014 Detailed characterization of particulates emitted by pre-commercial single-cylinder gasoline compression ignition engine *Combust. Flame* **161** 2151–64

Zhang A, Xu L, Sandison G and Cheng S 2006 Morphological study of endothelial cells during freezing *Phys. Med. Biol.* **51** 6047

Zhang R, Khalizov A F, Pagels J, Zhang D, Xue H and McMurry P H 2008 Variability in morphology, hygroscopicity, and optical properties of soot aerosols during atmospheric processing *Proc. Natl Acad. Sci. USA* **105** 10291–6

Zijlstra G S, Hinrichs W L J, Boer A H D and Frijlink H W 2004 The role of particle engineering in relation to formulation and de-agglomeration principle in the development of a dry powder formulation for inhalation of cetrorelix *Eur. J. Pharmaceutical Sci.* **23** 139–49

Zuberi B, Johnson K S, Aleks G K, Molina L T, Molina M J and Laskin A 2005 Hydrophilic properties of aged soot *Geophys. Res. Lett.* **32** L01807